International Journal on Magnetic Particle Imaging
Vol 7, No 1, Article ID 2103003, 6 Pages

Infinite Science Publishing

Research Article

Synomag®: The new high-performance tracer for magnetic particle imaging

P. Vogel[a*] · T. Kampf[a,c] · M.A. Rückert[a] · C. Grüttner[b] · A. Kowalski[b] · H. Teller[b] · V.C. Behr[a]

[a]Department of Experimental Physics 5 (Biophysics), University of Würzburg, Würzburg, Germany
[b]micromod Partikeltechnologie GmbH, Rostock, Germany
[c]Institute of Diagnostic and Interventional Neuroradiology, University Hospital Würzburg, Würzburg, Germany
*Corresponding author, email: Patrick.Vogel@physik.uni-wuerzburg.de

Received 14 January 2020; Accepted 12 March 2021; Published online 29 March 2021

Abstract

The success of tracer-based tomographic methods, such as Magnetic Particle Imaging (MPI), depends on two factors primarily: scanner hardware and tracer performance. Within the last years, several hardware improvements have been presented improving temporal and spatial resolution of MPI systems. However, there was still a lack of efficient commercially available tracers for MPI. Here we report on synomag® particles as a new tracer tailored for MPI, which shows almost four-times higher signal in a Traveling Wave MPI scanner than the established tracer Resovist®.

I. Introduction

Magnetic Particle Imaging (MPI) is a promising imaging modality for multiple applications in biology, chemistry, geology and medicine [1–5]. It is based on the nonlinear magnetization response of superparamagnetic iron-oxide nanoparticles (SPIONs) to time varying magnetic fields. For imaging, a field-free point (FFP) [1, 6–8] or field-free line (FFL) [9–12] generated by a strong magnetic field gradient is rapidly moved through the volume of interest to successively acquire signal in the vicinity of the FFP or FFL. This signal is processed for the visualization of the distribution of the magnetic material [13–16].

As a tracer-based imaging modality, the performance and success of MPI systems strongly depends on the scanner hardware and the tracer itself, as indicated by

$$FWHM \propto \frac{T}{G\,D^3\,M_S} \tag{1}$$

with the temperature T, gradient strength G of the MPI scanner, the core-diameter D of spherical particles, and the saturation magnetization M_S [6, 16]. Several developments in scanner hardware as well as sequence design introduced over the last years [2, 17, 18] lead to decreased scanning time [19, 20], enhanced signal sensitivity [21] and better spatial resolution [22]. Only few novel approaches in tracer development with high gain can be found [23–27].

For example, iron oxide dextran composite particles perimag® were applied as MPI tracers for in-vivo tracking and quantification of inhaled aerosol [5] and for quantitative MPI monitoring of the transplantation, biodistribution, and clearance of stem cells in-vivo [28]. In addition, only few commercial and (pre-)clinically approved particle systems are available [19], which are required for future MPI applications [20, 29].

In this study, a novel high-performance tracer for MPI (synomag®, micromod, Germany) [30] is characterized and compared to the established tracer Resovist® (Bayer, Germany) [31, 32] using Traveling Wave MPI (TWMPI) [7].

II. Materials and Methods

The requirement for an ideal MPI tracer is to provide a high signal as well as a good spatial resolution using small particles for *in-vivo* experiments often biologically tailored to specific applications, i.e., cell uptake or blood circulation [33]. This leads to high sensitivity [21] and high spatial resolution [22].

As indicated in (1), by increasing the iron oxide core diameter D of the tracer material, the resolution *FWHM* (Full Width at Half Maximum) is improved dramatically. Unfortunately, several limitations prevent this improvement. First is the particle core itself: to preserve a high magnetic moment within a single particle, only a single Weiss area (magnetic domain) is desirable. Above a certain particle size (~ 50 nm) it is energetically more efficient to form multiple domains, which also decreases the total magnetization [34]. In addition, relaxation effects, such as Néel- and Brown-Relaxation, increase with particle size and cause blurring artifacts and signal drops in MPI [35–38].

In theory, the ideal MPI tracer should have a magnetic core diameter of approx. 20-25 nm for a 25 kHz excitation field frequency and be monodisperse [39]. However, the major particle core size of Resovist® is about 4.2 nm [40], but the performance is impressive especially because only 3 percent of the particles contribute to the MPI signal, the agglomerated fraction (multi-core) with a second size distribution in the range of 25 nm [1, 41].

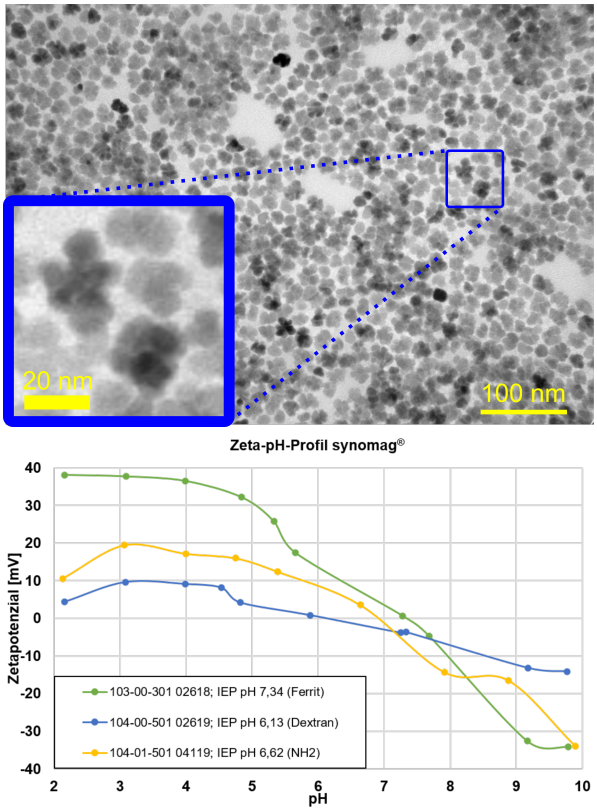

Figure 1: **Top:** Transmission electron microscopy (TEM) image of synomag® particles. **Bottom:** Comparison of zeta-potential-pH functions of synomag® and synomag®-D particles.

II.I. High performance tracer

The new synomag®-particles are multi-core particles featuring a nanoflower substructure of iron oxide crystallites (Figure 1) along with an excellent biocompatibility [30, 42].

The particles are synthesized by a polyol method via thermal decomposition of a suitable iron precursor [43, 44]. The nanoflower-shaped iron oxide cores (synomag®) are coated with dextran (mean weight: 40 kDa) to obtain biocompatible core-shell synomag®-D nanoparticles. The dextran shell covers the iron oxide core to improve the colloidal stability and to prevent aggregation especially in physiological buffers, e.g., TRIS, HEPES or PBS. The polysaccharide coating reduces redox-reactive effects at in-vitro and in-vivo applications. The coating with dextran leads to a shift of the amount of zeta-potential of the initial iron oxide nanoflower particles to neutral values over the whole pH range. Furthermore, the dextran shell provides a platform for specific functionalization and conjugation of target molecules.

II.II. Traveling Wave MPI

The TWMPI scanner [7, 18] offers a high flexibility in gradient strength [22], temporal resolution [45] and scanning modes [17].

For comparison, the synomag®(-D) and Resovist® samples were measured under same conditions for generating all data sets: 2D-slice-scanning mode (SSM)n [3] was used operating at frequencies $f_1 = 1050$ Hz and $f_2 = 12150$ Hz and scanning a FOV of 65 mm in length and 29 mm in diameter with a gradient strength of 1.5 T/m (magnetic field amplitude of about 35 mT for the dLGA and about 45 mT for deflection coil). The total acquisition time for each image was 200 ms with 10 averages.

For signal-to-noise (SNR) determination, the datasets were Fourier transformed and the magnitude of the harmonic at $f_{\text{peak}} = 47.55$ kHz (first left-handed sideband-harmonic of the fourth higher harmonic of f_{p2}: $f_{\text{peak}} = 4f_2 - f_1$) was evaluated (see Figure 2). For image reconstruction, a standard Wiener filter with an appropriate point-spread-function (PSF) was applied to the re-gridded raw-images [3, 13, 14].

II.III. Sample Preparation

Two dilution series have been prepared for each particle system starting with a defined amount of buffer (NaCl solution 0.9 %) to which the desired amount of particle solution has been added resulting in a defined target

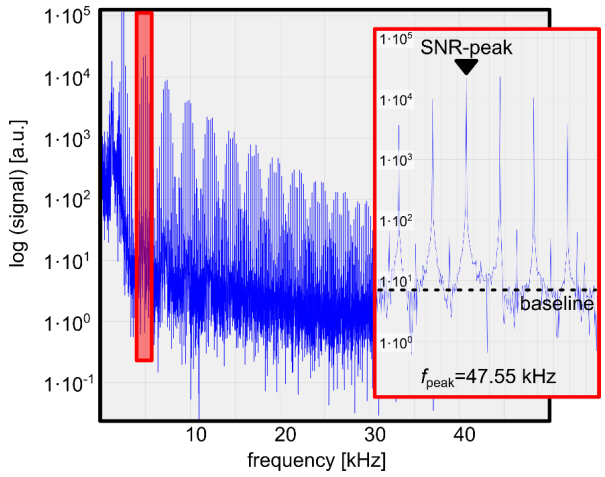

Figure 2: SNR calculation based on a single peak within a full spectrum. The SNR is the difference between the amplitude of the absolute spectrum at the baseline signal.

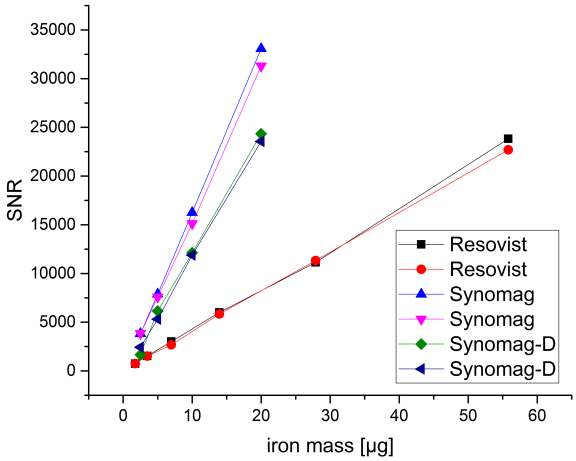

Figure 3: Graphical results of the SNR measurements: the SNR depending on the iron mass.

volume of 100 μl for dilution factor of 1:5, 1:10, and 1:20, a target volume of 200 μl for 1:40, and a target volume of 400 μl for 1:80.

III. Results

In Table 1 an overview of the results of the measured samples is given. The samples were prepared with two dilution series of each particle system (Resovist®, synomag® and synomag®-D) and measured with the same volume size. For comparison, the measured SNR of every sample is normalized to the iron mass of every particle system (based on the originating concentration). By determining an average value of the SNR/g Fe, the signal strength of synomag® (synomag®: LOT-01719103-02, synomag®-D: LOT-0219104-02) is about four times higher than that of Resovist®.

Table 1: Overview about the values from different particle samples: synomag®(-D) (micromod, Germany, conc. 5 mg Fe/ml) and Resovist® (Bayer, Germany, conc. 27.5 mg Fe/ml). (*) The SNR value is taken from the magnitude of the Fourier transformed at frequency $f_{peak} = 47.55$ kHz.

Sample	Dilution factor	Volume [μl]	Iron mass [μg]	SNR (*)	SNR /μg Fe
synomag	1:5	20	20	33072	1564
synomag	1:10	20	10	16250	1625
synomag	1:20	20	5	7880	1576
synomag	1:40	20	2.5	3840	1532
synomag-D	1:5	20	20	24331	1217
synomag-D	1:10	20	10	12125	1213
synomag-D	1:20	20	5	6146	1229
synomag-D	1:40	20	2.5	3840	1220
Resovist	1:10	20	55.8	23830	427
Resovist	1:20	20	27.9	11136	399
Resovist	1:40	20	13.9	6003	430
Resovist	1:80	20	7.0	3010	431

Table 2: Results of the linear regression of the measured samples (see Figure 3).

particle sytem	slope	intercept
Resovist® #1	423±8	0.99869
Resovist® #2	406±3	0.99981
synomag® #1	1674±6	0.99997
synomag® #2	1572±21	0.99964
synomag®-D #1	1268±52	0.99659
synomag®-D #2	1211±21	0.99939

In Figure 3 the graphical results of the SNR comparison measurements are shown. The synomag® particles show the highest SNR dependency on the iron mass (Figure 3 left). By normalizing the SNR on the iron mass (SNR/g Fe), the signals of the different particle systems are comparable. The synomag® and synomag®-D tracer show an almost four respectively three times higher signal gain than Resovist® (see Table 1).

In Figure 4 a selection of raw-images (left) and reconstructed images (right) for synomag® and Resovist® of single point samples are given [3]. In all cases the signal is sufficiently strong to reconstruct the point sample clearly. The width of the PSF for synomag® is narrower although the iron mass is less because of the higher SNR over the complete spectrum resulting in a better resolution [6, 22].

IV. Discussion

Since the first publication of Magnetic Particle Imaging [1], several different types of MPI scanners have been established [2]. The presented results are expected to be

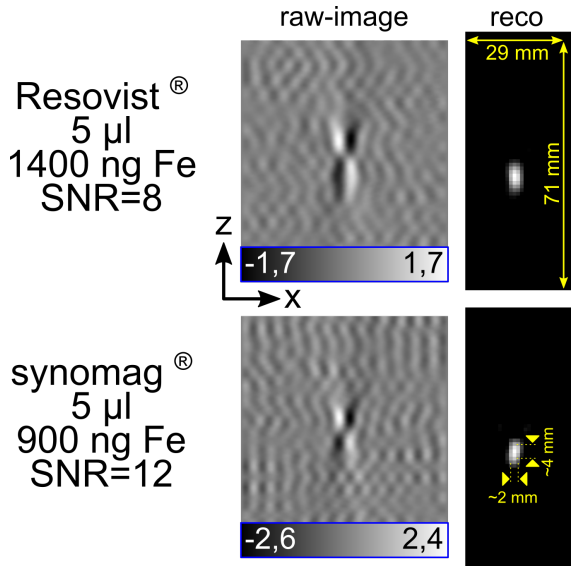

Figure 4: Results of the imaging experiments with two point-like samples: **Left:** the point-spread-function (raw-image). **Right:** the reconstructed images.

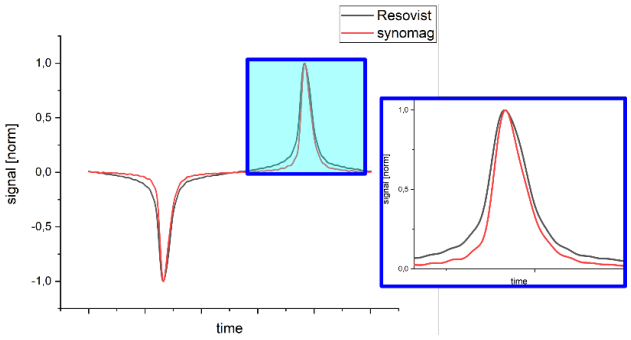

Figure 5: **Top:** Normalized time signals over one period of the excitation frequency $f_{\mathrm{MPS}} = 19.95$ kHz of Magnetic Particle Spectrometer (MPS) measurements at 41 mT. The signal from synomag® (iron conc. of 5 mg/ml) shows a slightly narrower point-spread-function (PSF) than the signal of Resovist® with iron conc. of 27.5 mg/ml. **Bottom:** Spectrum of both particle systems: the Resovist® particle system consists of two particle size distributions, which can be seen as two different slopes of the harmonic amplitudes.

valid for other MPI scanner types since the basic signal generation is common to all of them.

In Figure 5 on the left graph, the normalized time signals of a Resovist® (conc. 27.5 mg Fe/ml) and synomag® (conc. 5 mg FE/ml) sample is shown, which have been measured with a home-built Magnetic Particle Spectrometer (MPS) device [46] operating at a frequency of $f_{\mathrm{MPS}} = 19.95$ kHz and a magnetic field amplitude of about 41 mT. In the zoomed in area, the relaxation effects can be seen in more detail, where synomag® shows a narrower peak width.

In Figure 5 right, the amplitudes of the Fourier-transformed signals of Resovist® and synomag® are shown. The spectrum of Resovist® exhibits clearly two different slopes of harmonic amplitudes, which is an indication of the presence of two different core diameter distribution sizes [47]. However, since mainly the larger particles generate the MPI/MPS signal [1], in case of Resovist®, the part of usable iron mass is less compared to synomag®.

However, until now the exact mechanism leading to the better performance of the synomag® particle system remains unexplained. In initial tests, for iron oxide-based nanoparticles a strong correlation between good performance in hyperthermia [48] and good imaging result in MPI [49] has been shown and nanoflower particles show outstanding results in hyperthermia [50, 51].

The dextran coating prevents interactions between the single iron oxide nanoflower cores and leads to a slight reduction of the MPI signal (see Table 1, Table 2 and Figure 3), but is crucial fpr colloidal stability and biocompatibility.

V. Conclusion

The superior performance of synomag®(-D) particles with an almost four- respectively three-times higher signal-to-noise ratio per mass iron compared to Resovist® using TWMPI technology is reported.

This sets the stage for the application specific surface design of synomag® particles meeting the requirements for further pre-clinical investigations.

Acknowledgments

C.G. and A.K. are employees and H.T. is the CEO of micromod Partikeltechnologie, GmbH the manufacturer of the nanoparticles used in this study. The authors declare that they have no known competing financial interests or personal relationships that could have appeared to influence the work reported in this paper. This work was partially supported by the German Research Council (DFG) under Grant BE 5293/1-1/2 and VO 2288/1-1.

References

[1] B. Gleich and J. Weizenecker. Tomographic imaging using the nonlinear response of magnetic particles. *Nature*, 435(7046):1214–1217, 2005, doi:10.1038/nature03808.

[2] T. Knopp, N. Gdaniec, and M. Möddel. Magnetic particle imaging: from proof of principle to preclinical applications. *Physics in Medicine & Biology*, 62(14):R124–R178, 2017, doi:10.1088/1361-6560/aa6c99.

[3] P. Vogel, M. A. Rückert, P. Klauer, W. H. Kullmann, P. M. Jakob, and V. C. Behr. First in vivo traveling wave magnetic particle imaging of a beating mouse heart. *Physics in Medicine and Biology*, 61(18):6620–6634, 2016, doi:10.1088/0031-9155/61/18/6620.

[4] S. Herz, P. Vogel, T. Kampf, P. Dietrich, S. Veldhoen, M. A. Rückert, R. Kickuth, V. C. Behr, and T. A. Bley. Magnetic Particle Imaging–Guided Stenting. *Journal of Endovascular Therapy*, 26(4):512–519, 2019, doi:10.1177/1526602819851202.

[5] Z. W. Tay, P. Chandrasekharan, X. Y. Zhou, E. Yu, B. Zheng, and S. Conolly. In vivo tracking and quantification of inhaled aerosol using magnetic particle imaging towards inhaled therapeutic monitoring. *Theranostics*, 8(13):3676–3687, 2018, doi:10.7150/thno.26608.

[6] P. W. Goodwill and S. M. Conolly. The X-Space Formulation of the Magnetic Particle Imaging Process: 1-D Signal, Resolution, Bandwidth, SNR, SAR, and Magnetostimulation. *IEEE Transactions on Medical Imaging*, 29(11):1851–1859, 2010, doi:10.1109/TMI.2010.2052284.

[7] P. Vogel, M. A. Rückert, P. Klauer, W. H. Kullmann, P. M. Jakob, and V. C. Behr. Traveling Wave Magnetic Particle Imaging. *IEEE Transactions on Medical Imaging*, 33(2):400–407, 2014, doi:10.1109/TMI.2013.2285472.

[8] P. Vogel, T. Kampf, S. Herz, M. A. Rückert, T. A. Bley, and V. C. Behr. Parallel magnetic particle imaging. *Review of Scientific Instruments*, 91(4):045117, 2020, doi:10.1063/1.5126108.

[9] J. Weizenecker, B. Gleich, and J. Borgert. Magnetic particle imaging using a field free line. *Journal of Physics D: Applied Physics*, 41(10):105009, 2008, doi:10.1088/0022-3727/41/10/105009.

[10] P. W. Goodwill, J. J. Konkle, B. Zheng, E. U. Saritas, and S. T. Conolly. Projection X-Space Magnetic Particle Imaging. *IEEE Transactions on Medical Imaging*, 31(5):1076–1085, 2012, doi:10.1109/TMI.2012.2185247.

[11] K. Bente, M. Weber, M. Graeser, T. F. Sattel, M. Erbe, and T. M. Buzug. Electronic Field Free Line Rotation and Relaxation Deconvolution in Magnetic Particle Imaging. *IEEE Transactions on Medical Imaging*, 34(2):644–651, 2015, doi:10.1109/TMI.2014.2364891.

[12] P. Vogel, J. Markert, M. A. Rückert, S. Herz, B. Keßler, K. Dremel, D. Althoff, M. Weber, T. M. Buzug, T. A. Bley, W. H. Kullmann, R. Hanke, S. Zabler, and V. C. Behr. Magnetic Particle Imaging meets Computed Tomography: first simultaneous imaging. *Scientific Reports*, 9(1):12627, 2019, doi:10.1038/s41598-019-48960-1.

[13] P. Vogel, T. Kampf, M. A. Rückert, and V. C. Behr. Flexible and Dynamic Patch Reconstruction for Traveling Wave Magnetic Particle Imaging. *International Journal on Magnetic Particle Imaging*, 2(2), 2016, doi:10.18416/IJMPI.2016.1611001.

[14] P. Vogel, S. Herz, T. Kampf, M. A. Rückert, T. A. Bley, and V. C. Behr. Low Latency Real-time Reconstruction for MPI Systems. *International Journal on Magnetic Particle Imaging*, 3(2), 2017, doi:10.18416/IJMPI.2017.1707002.

[15] S. Ilbey, C. B. Top, A. Güngör, T. Çukur, E. U. Saritas, and H. E. Güven. Comparison of System-Matrix-Based and Projection-Based Reconstructions for Field Free Line Magnetic Particle Imaging. *International Journal on Magnetic Particle Imaging*, 3(1), 2017, doi:10.18416/IJMPI.2017.1703022.

[16] J. Rahmer, J. Weizenecker, B. Gleich, and J. Borgert. Signal encoding in magnetic particle imaging: properties of the system function. *BMC Medical Imaging*, 9:4, 2009, doi:10.1186/1471-2342-9-4.

[17] P. Vogel, M. A. Rückert, P. Klauer, S. Herz, T. Kampf, T. A. Bley, and V. C. Behr. Real-time 3D Dynamic Rotating Slice-Scanning Mode for Traveling Wave MPI. *International Journal on Magnetic Particle Imaging*, 3(2), 2017, doi:10.18416/IJMPI.2017.1706001.

[18] P. Vogel, P. Klauer, M. A. Ruckert, T. A. Bley, W. H. Kullmann, P. M. Jakob, and V. C. Behr. Dynamic Linear Gradient Array for Traveling Wave Magnetic Particle Imaging. *IEEE Transactions on Magnetics*, 54(2):1–9, 2018, doi:10.1109/TMAG.2017.2764440.

[19] J. W. Bulte. Superparamagnetic iron oxides as MPI tracers: A primer and review of early applications. *Advanced Drug Delivery Reviews*, 138:293–301, 2019, doi:10.1016/j.addr.2018.12.007.

[20] E. E. Mason, C. Z. Cooley, S. F. Cauley, M. A. Griswold, S. M. Conolly, and L. L. Wald. Design analysis of an MPI human functional brain scanner. *International Journal on Magnetic Particle Imaging*, 3(1), 2017, doi:10.18416/IJMPI.2017.1703008.

[21] M. Graeser, T. Knopp, P. Szwargulski, T. Friedrich, A. von Gladiss, M. Kaul, K. M. Krishnan, H. Ittrich, G. Adam, and T. M. Buzug. Towards Picogram Detection of Superparamagnetic Iron-Oxide Particles Using a Gradiometric Receive Coil. *Scientific Reports*, 7(1):6872, 2017, doi:10.1038/s41598-017-06992-5.

[22] P. Vogel, M. A. Ruckert, S. J. Kemp, A. P. Khandhar, R. M. Ferguson, S. Herz, A. Vilter, P. Klauer, T. A. Bley, K. M. Krishnan, and V. C. Behr. Micro-Traveling Wave Magnetic Particle Imaging—Sub-Millimeter Resolution With Optimized Tracer LS-008. *IEEE Transactions on Magnetics*, 55(10):1–7, 2019, doi:10.1109/TMAG.2019.2924198.

[23] R. M. Ferguson, K. R. Minard, A. P. Khandhar, and K. M. Krishnan. Optimizing magnetite nanoparticles for mass sensitivity in magnetic particle imaging. *Medical Physics*, 38(3):1619–1626, 2011, doi:10.1118/1.3554646.

[24] F. Ludwig, D. Eberbeck, N. Löwa, U. Steinhoff, T. Wawrzik, M. Schilling, and L. Trahms. Characterization of magnetic nanoparticle systems with respect to their magnetic particle imaging performance. *Biomedizinische Technik/Biomedical Engineering*, 58(6), 2013, doi:10.1515/bmt-2013-0013.

[25] D. Eberbeck, C. L. Dennis, N. F. Huls, K. L. Krycka, C. Gruttner, and F. Westphal. Multicore Magnetic Nanoparticles for Magnetic Particle Imaging. *IEEE Transactions on Magnetics*, 49(1):269–274, 2013, doi:10.1109/TMAG.2012.2226438.

[26] H. Kratz, M. Taupitz, A. Ariza de Schellenberger, O. Kosch, D. Eberbeck, S. Wagner, L. Trahms, B. Hamm, and J. Schnorr. Novel magnetic multicore nanoparticles designed for MPI and other biomedical applications: From synthesis to first in vivo studies. *PLOS ONE*, 13(1):e0190214R. Levy, Ed., 2018, doi:10.1371/journal.pone.0190214.

[27] H. Kratz, A. Mohtashamdolatshahi, D. Eberbeck, O. Kosch, R. Hauptmann, F. Wiekhorst, M. Taupitz, B. Hamm, and J. Schnorr. MPI Phantom Study with A High-Performing Multicore Tracer Made by Coprecipitation. *Nanomaterials*, 9(10):1466, 2019, doi:10.3390/nano9101466.

[28] B. Zheng, M. P. von See, E. Yu, B. Gunel, K. Lu, T. Vazin, D. V. Schaffer, P. W. Goodwill, and S. M. Conolly. Quantitative Magnetic Particle Imaging Monitors the Transplantation, Biodistribution, and Clearance of Stem Cells In Vivo. *Theranostics*, 6(3):291–301, 2016, doi:10.7150/thno.13728.

[29] M. Graeser, F. Thieben, P. Szwargulski, F. Werner, N. Gdaniec, M. Boberg, F. Griese, M. Möddel, P. Ludewig, D. van de Ven, O. M. Weber, O. Woywode, B. Gleich, and T. Knopp. Human-sized magnetic particle imaging for brain applications. *Nature Communications*, 10(1):1936, 2019, doi:10.1038/s41467-019-09704-x.

[30] C. Grüttner, A. Kowalski, F. Fidler, M. Steinke, F. Westphal, and H. Teller, synomag® nanoflower particles: A new tracer for mpi, physical characterization and initial in vitro toxicity studies, in *International Workshop on Magnetic Particle Imaging*, 17–18, 2018.

[31] R. Lawaczeck, H. Bauer, T. Frenzel, M. Hasegawa, Y. Ito, K. Kito, N. Miwa, H. Tsutsui, H. Vogler, and H.-J. Weinmann. Magnetic Iron Oxide Particles Coated with Carboxydextran for Parenteral Administration and Liver Contrasting. *Acta Radiologica*, 38(4):584–597, 1997, doi:10.1080/02841859709174391.

[32] P. Reimer and T. Balzer. Ferucarbotran (Resovist): a new clinically approved RES-specific contrast agent for contrast-enhanced MRI of the liver: properties, clinical development, and applications. *European Radiology*, 13(6):1266–1276, 2003, doi:10.1007/s00330-002-1721-7.

[33] Q. Feng, Y. Liu, J. Huang, K. Chen, J. Huang, and K. Xiao. Uptake, distribution, clearance, and toxicity of iron oxide nanoparticles with different sizes and coatings. *Scientific Reports*, 8(1):2082, 2018, doi:10.1038/s41598-018-19628-z.

[34] E. Kneller, A. Seeger, and H. Kronmüller, Ferromagnetismus. Berlin, Heidelberg: Springer Berlin Heidelberg, 1962, doi:10.1007/978-3-642-86695-1.

[35] P. W. Goodwill, K. Lu, B. Zheng, and S. M. Conolly. An x-space magnetic particle imaging scanner. *Review of Scientific Instruments*, 83(3):033708, 2012, doi:10.1063/1.3694534.

[36] J. Dieckhoff, D. Eberbeck, M. Schilling, and F. Ludwig. Magnetic-field dependence of Brownian and Néel relaxation times. *Journal of Applied Physics*, 119(4):043903, 2016, doi:10.1063/1.4940724.

[37] S. A. Shah, D. B. Reeves, R. M. Ferguson, J. B. Weaver, and K. M. Krishnan. Mixed Brownian alignment and Néel rotations in superparamagnetic iron oxide nanoparticle suspensions driven by an ac field. *Physical Review B*, 92(9):094438, 2015, doi:10.1103/PhysRevB.92.094438.

[38] R. J. Deissler, Y. Wu, and M. A. Martens. Dependence of Brownian and Néel relaxation times on magnetic field strength. *Medical Physics*, 41(1):012301, 2013, doi:10.1118/1.4837216.

[39] R. M. Ferguson, A. P. Khandhar, H. Arami, L. Hua, O. Hovorka, and K. M. Krishnan. Tailoring the magnetic and pharmacokinetic properties of iron oxide magnetic particle imaging tracers. *Biomedizinische Technik/Biomedical Engineering*, 58(6), 2013, doi:10.1515/bmt-2012-0058.

[40] L. M. Bauer, S. F. Situ, M. A. Griswold, and A. C. S. Samia. Magnetic Particle Imaging Tracers: State-of-the-Art and Future Directions. *The Journal of Physical Chemistry Letters*, 6(13):2509–2517, 2015, doi:10.1021/acs.jpclett.5b00610.

[41] D. Eberbeck, F. Wiekhorst, S. Wagner, and L. Trahms. How the size distribution of magnetic nanoparticles determines their magnetic particle imaging performance. *Applied Physics Letters*, 98(18):182502, 2011, doi:10.1063/1.3586776.

[42] C. Matschegewski, A. Kowalski, K. Müller, H. Teller, N. Grabow, S. Großmann, K.-P. Schmitz, and S. Siewert. Biocompatibility of magnetic iron oxide nanoparticles for biomedical applications. *Current Directions in Biomedical Engineering*, 5(1):573–576, 2019, doi:10.1515/cdbme-2019-0144.

[43] L. Lartigue, P. Hugounenq, D. Alloyeau, S. P. Clarke, M. Lévy, J.-C. Bacri, R. Bazzi, D. F. Brougham, C. Wilhelm, and F. Gazeau. Cooperative Organization in Iron Oxide Multi-Core Nanoparticles Potentiates Their Efficiency as Heating Mediators and MRI Contrast Agents. *ACS Nano*, 6(12):10935–10949, 2012, doi:10.1021/nn304477s.

[44] P. Bender, J. Fock, C. Frandsen, M. F. Hansen, C. Balceris, F. Ludwig, O. Posth, E. Wetterskog, L. K. Bogart, P. Southern, W. Szczerba, L. Zeng, K. Witte, C. Grüttner, F. Westphal, D. Honecker, D. González-Alonso, L. Fernández Barquín, and C. Johansson. Relating Magnetic Properties and High Hyperthermia Performance of Iron Oxide Nanoflowers. *The Journal of Physical Chemistry C*, 122(5):3068–3077, 2018, doi:10.1021/acs.jpcc.7b11255.

[45] P. Vogel, M. A. Ruckert, T. Kampf, S. Herz, A. Stang, L. Wockel, T. A. Bley, S. Dutz, and V. C. Behr. Superspeed Bolus Visualization for Vascular Magnetic Particle Imaging. *IEEE Transactions on Medical Imaging*, 39(6):2133–2139, 2020, doi:10.1109/TMI.2020.2965724.

[46] S. Biederer, T. Knopp, T. F. Sattel, K. Lüdtke-Buzug, B. Gleich, J. Weizenecker, J. Borgert, T. M. Buzug, and K. Lüdtke-Buzug. Magnetization response spectroscopy of superparamagnetic nanoparticles for magnetic particle imaging. *Journal of Physics D: Applied Physics*, 42(20):205007, 2009, doi:10.1088/0022-3727/42/20/205007.

[47] T. Yoshida, T. Nakamura, O. Higashi, and K. Enpuku. Magnetic fractionation and characterization of magnetic nanoparticles for magnetic particle imaging. *Japanese Journal of Applied Physics*, 57(8):080302, 2018, doi:10.7567/JJAP.57.080302.

[48] M. Shinkai. Functional magnetic particles for medical application. *Journal of Bioscience and Bioengineering*, 94(6):606–613, 2002, doi:10.1016/S1389-1723(02)80202-X.

[49] P. Southern, J. Wells, U. Steinhoff, F. Wiekhorst, C. Jonasson, C. Johansson, and Q. Pankhurst, Oberservation of correlated magnetic particle imaging and magnetic hyperthermia metrics in iron oxide nanoparticles, in *International Workshop on Magnetic Particle Imaging*, 2019.

[50] H. Gavilán, E. H. Sánchez, M. E. F. Brollo, L. Asín, K. K. Moerner, C. Frandsen, F. J. Lázaro, C. J. Serna, S. Veintemillas-Verdaguer, M. P. Morales, and L. Gutiérrez. Formation Mechanism of Maghemite Nanoflowers Synthesized by a Polyol-Mediated Process. *ACS Omega*, 2(10):7172–7184, 2017, doi:10.1021/acsomega.7b00975.

[51] H. Gavilán, A. Kowalski, D. Heinke, A. Sugunan, J. Sommertune, M. Varón, L. K. Bogart, O. Posth, L. Zeng, D. González-Alonso, C. Balceris, J. Fock, E. Wetterskog, C. Frandsen, N. Gehrke, C. Grüttner, A. Fornara, F. Ludwig, S. Veintemillas-Verdaguer, C. Johansson, and M. P. Morales. Colloidal Flower-Shaped Iron Oxide Nanoparticles: Synthesis Strategies and Coatings. *Particle & Particle Systems Characterization*, 34(7):1700094, 2017, doi:10.1002/ppsc.201700094.

